

# Probing the density dependence of the symmetry energy with central heavy ion collisions

XIE Wenjie<sup>1,2,3</sup> ZHANG Fengshou<sup>1,2,4,\*</sup>

<sup>1</sup>The Key Laboratory of Beam Technology and Material Modification of Ministry of Education, College of Nuclear Science and Technology, Beijing Normal University, Beijing 100875, China

<sup>2</sup>Beijing Radiation Center, Beijing 100875, China

<sup>3</sup>Department of Physics, Yuncheng University, Yuncheng 044000, China

<sup>4</sup>Center of Theoretical Nuclear Physics, National Laboratory of Heavy Ion Accelerator of Lanzhou, Lanzhou 730000, China

**Abstract** An improved isospin dependent Boltzmann Langevin model, in which the inelastic channels and momentum dependent interactions are incorporated, is used to investigate the high-density behavior of nuclear symmetry energy. By taking several forms of nuclear symmetry energy, we calculate the time evolutions of neutron over proton ratio,  $\pi$  multiplicity and  $\pi^-/\pi^+$  ratio, and the kinetic energy and transverse momentum spectra of  $\pi^-/\pi^+$  ratio in the heavy ion collisions at 400A MeV. It is found that the neutron over proton ratio and  $\pi^-/\pi^+$  ratio are very sensitive to the nuclear symmetry energy, and the  $\pi^-$  is more sensitive to the nuclear symmetry energy than the  $\pi^+$ . A supersoft symmetry energy results in a larger  $\pi^-/\pi^+$  ratio.

**Key words** Improved isospin dependent Boltzmann-Langevin model, Nuclear symmetry energy, Neutron over proton ratio, Pion production

## 1 Introduction

Constraints on the nuclear symmetry energy  $E_{\text{sym}}(\rho)$  have been an very interesting subject in the last few years. The  $E_{\text{sym}}(\rho)$  which is an estimate of the energy cost to convert all protons to neutrons at the fixed density in the symmetric nuclear matter, is very important both in nuclei, such as the binding energy, and in neutron stars, such as the nature and stability of the phases within the star<sup>[1,2]</sup>. The energy per nucleon in asymmetric nuclear matter can usually be expressed as

$$E(\rho, \delta) = E(\rho, \delta = 0) + E_{\text{sym}}(\rho)\delta^2 + O(\delta^4), \quad (1)$$

where  $\delta = (\rho_n - \rho_p)/\rho$  and  $\rho_n$ ,  $\rho_p$  and  $\rho$  are the neutron, proton and total nucleon densities, respectively. The first term in Eq.(1) is the symmetric contribution and the second term is the symmetry energy contribution. The higher-order terms  $O(\delta^4)$  in  $\delta$  are commonly negligible<sup>[3]</sup>. Generally, there are

two forms of  $E_{\text{sym}}(\rho)$  predicted by various theoretical models. The one is that the  $E_{\text{sym}}(\rho)$  increases with the increasing nucleon density and the other is that  $E_{\text{sym}}(\rho)$  increases up to the saturation density  $\rho_0$  and then decreases with the increasing density.

At supra-saturation densities ( $\rho > \rho_0$ ), the form of the  $E_{\text{sym}}(\rho)$  is very controversial. Even the trend of the  $E_{\text{sym}}(\rho)$  with increasing density is not constrained yet. A lot of probes have been proposed to constrain the  $E_{\text{sym}}(\rho)$  at supra-saturation density, such as the neutron over proton ratio of squeezed-out nucleons<sup>[4]</sup>, the neutron-proton differential flow<sup>[5]</sup>, the  $\pi^-/\pi^+$  ratio<sup>[6-10]</sup>, the  $K^0/K^+$  ratio<sup>[10]</sup>, the  $\Sigma^-/\Sigma^+$  ratio<sup>[11]</sup> and so on. Among above probes, the  $\pi^-/\pi^+$  ratio as a promising one is motivated by the  $\Delta(1232)$  resonance model<sup>[12]</sup>, in which a primordial relation between  $\pi^-/\pi^+$  ratio and  $N/Z$  is predicted. That is

$$\pi^-/\pi^+ = (5N^2 + NZ)/(5Z^2 + NZ) \approx (N/Z)^2, \quad (2)$$

where the  $N$  and  $Z$  are the neutron and proton

Supported by National Natural Science Foundation of China (NSFC) projects (Nos. 11025524 and 11161130520) and National Basic Research Program of China (No. 2010CB832903).

\* Corresponding author. E-mail address: fszhang@bnu.edu.cn

Received date: 2013-06-27

numbers in the participant region of the reaction. The  $N/Z$  is determined by the  $E_{\text{sym}}(\rho)$  by the dynamical isospin fractionation<sup>[6]</sup>. Therefore, one can use the  $\pi^-/\pi^+$  ratio to constrain the  $E_{\text{sym}}(\rho)$ .

Using the  $\pi^-/\pi^+$  ratio as a probe of the  $E_{\text{sym}}(\rho)$ , a larger uncertainty exists. By comparing with the FOPI data<sup>[15]</sup>, a very soft  $E_{\text{sym}}(\rho)$  was suggested by the isospin-dependent Boltzmann Uehling Uhlenbeck model (IBUU04)<sup>[7]</sup> and improved isospin dependent Boltzmann Langevin model (ImIBL)<sup>[9]</sup>, and a hard  $E_{\text{sym}}(\rho)$  was suggested by the improved isospin dependent quantum molecular dynamics model (ImIQMD)<sup>[8]</sup>.

At sub-saturation densities ( $\rho < \rho_0$ ), the trend of the  $E_{\text{sym}}(\rho)$  with increasing density is almost constrained but the quantitative results are not obtained yet. There are also a lot of probes to constrain the  $E_{\text{sym}}(\rho)$  in sub-saturation density region, such as the isospin diffusion<sup>[14,15]</sup>, the neutron skin thickness<sup>[16]</sup>, the single and double neutron over proton ratios<sup>[14,17-20]</sup>, the heavy fragment mass distribution<sup>[21]</sup> and so on. The IBUU04 model<sup>[15]</sup> suggested an almost linear  $E_{\text{sym}}(\rho)$  by analyzing the isospin diffusion data. Also the constrained molecular dynamics II model (CoMDII) suggested a linear one by calculating the heavy fragment mass distribution<sup>[21]</sup>. However, the improved quantum molecular dynamics model (ImQMD)<sup>[14]</sup> and the isospin dependent quantum molecular dynamics model (IQMD)<sup>[17]</sup> predicted a soft  $E_{\text{sym}}(\rho)$  by analyzing the double neutron over proton ratio. Recently, a quantum statistical approach predicted the  $E_{\text{sym}}(\rho)$  at low temperature and low density limit<sup>[22]</sup>.

As a kind of ensemble-averaged theory, the usual BUU model have been very successful in describing the various phenomena in heavy ion collisions. However, the fluctuations, which are very important in preequilibrium particle emission, subthreshold particle production and multifragmentation are not included in the BUU model. In the QMD-like model which is a kind of many-body theory, the reactions are simulated event by event. Though the fluctuations are realized in the QMD simulations, the correlations among the events are uncertain. Moreover, the QMD model fails to explain the subthreshold kaon production<sup>[23]</sup>.

In this paper, we will use the ImIBL model to investigate the  $E_{\text{sym}}(\rho)$  using the neutron over proton ratio and  $\pi^-/\pi^+$  ratio in the  $^{48}\text{Ca}+^{48}\text{Ca}$  collisions at 400A MeV. The paper is organized as follows. We introduce our model in Section 2. The calculated results are given in Section 3. Finally, we will give some conclusions.

## 2 Theoretical model

The ImIBL model used in this paper is an updated version of the Boltzmann-Langevin model(BL)<sup>[24]</sup>. According to the BL model, the fluctuating phase space single particle density fulfills the following equation<sup>[24]</sup>:

$$\left( \frac{\partial}{\partial t} + \frac{\vec{p}}{m} \cdot \nabla_r - \nabla_r U(\hat{f}) \cdot \nabla_p \right) \hat{f}(\vec{r}, \vec{p}, t) = K(\hat{f}) + \delta K(\vec{r}, \vec{p}, t). \quad (3)$$

The left-hand side describes the Vlasov propagation determined by nuclear mean field  $U(\hat{f})$ .  $K(\hat{f})$  is the collision term of the usual BUU form but is characterized by the fluctuating density  $\hat{f}(\vec{r}, \vec{p}, t)$ .  $\delta K(\vec{r}, \vec{p}, t)$  is the fluctuating collision term, which can be explained as a stochastic force acting on the  $\hat{f}(\vec{r}, \vec{p}, t)$ , and is characterized by the following correlation function:

$$\langle \delta K(\vec{r}_1, \vec{p}_1, t_1) \delta K(\vec{r}_2, \vec{p}_2, t_2) \rangle = C(\vec{p}_1, \vec{p}_2) \delta(\vec{r}_1 - \vec{r}_2) \delta(t_1 - t_2), \quad (4)$$

where the angle brackets denote a local average, performed over fluctuating densities generated during a time interval  $\delta t$ . The correlation function  $C(\vec{p}_1, \vec{p}_2)$  can be reduced and expressed as in the weak-coupling limit and determined by the one-body properties of the locally averaged distribution as indicated in Ref.[25]. The numerical simulation method used in BL model is the projection method<sup>[24,25]</sup> which projects the fluctuations on a set of low order local multipole moments  $Q_{LM}$  of order  $L$  with magnetic quantum numbers  $M$  of the momentum distribution. The fluctuations of these multipole moments can be characterized by a diffusion matrix and can be deduced from the correlation matrix  $C(\vec{p}, \vec{p}')$  as<sup>[25]</sup>

$$\begin{aligned}
 C_{LML'M'}(\vec{r}, t) &= \int d\vec{p}d\vec{p}' Q_{LM}(\vec{p}) Q_{L'M'}(\vec{p}') C(\vec{p}, \vec{p}') \\
 &= \int d\vec{p}_1 d\vec{p}_2 d\vec{p}_3 d\vec{p}_4 \Delta Q_{LM} \Delta Q_{L'M'} \\
 &\quad \times W(12, 34) f_1 f_2 (1-f_3)(1-f_4)
 \end{aligned} \quad (5)$$

with

$$\Delta Q_{LM} = Q_{LM}(\vec{p}_1) + Q_{LM}(\vec{p}_2) - Q_{LM}(\vec{p}_3) - Q_{LM}(\vec{p}_4).$$

According to the Refs.[24-27], the stochastic component of the dynamics can be reduced to the following two equations:

$$\begin{aligned}
 \hat{Q}_{20}(\vec{r}, t + \delta t) &= Q_2(\vec{r}, t + \delta t) + \sqrt{\delta t} C_2(\vec{r}, t) W_2, \\
 \hat{Q}_{30}(\vec{r}, t + \delta t) &= Q_3(\vec{r}, t + \delta t) + \sqrt{\delta t} C_3(\vec{r}, t) W_3,
 \end{aligned} \quad (6)$$

where  $W_2$  and  $W_3$  are Gaussian random numbers. The  $\hat{Q}_{20}$  and  $\hat{Q}_{30}$  are the fluctuating quadrupole and octupole moments. The fluctuations are inserted into the momentum space through a scaling procedure as indicated in Ref.[25].

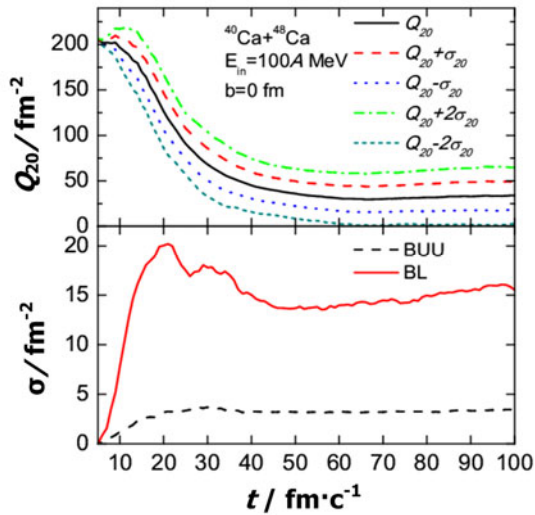


**Fig.1** (Color online) Time evolution of the ensemble-averaged quadrupole moment  $Q_{20}$ ,  $Q_{20} \pm \sigma_{20}$  and  $Q_{20} \pm 2\sigma_{20}$  of the momentum distribution in the ImIBL model (upper) and the associated variance  $\sigma_{20}$  (bottom) for central  $^{40}\text{Ca}+^{48}\text{Ca}$  collisions at  $100A$  MeV.

In Fig.1, we show the time evolution of the ensemble-averaged total quadrupole moment  $Q_{20}$ ,  $Q_{20} \pm \sigma_{20}$  and  $Q_{20} \pm 2\sigma_{20}$  of the momentum distribution and the associated variance  $\sigma_{20}$  from central  $^{40}\text{Ca}+^{48}\text{Ca}$  collisions at  $100A$  MeV in the ImIBL and BUU models, where  $\sigma_{20} = \sqrt{\langle Q_{20}^2 \rangle - \langle Q_{20} \rangle^2}$  is the standard deviation function. For a Gaussian distribution,  $Q_{20} \pm \sigma_{20}$  and  $Q_{20} \pm 2\sigma_{20}$  correspond to

84.3 and 99.5 percent of the number of events respectively<sup>[27]</sup>. From the upper panel of Fig.1, we can see that the  $Q_{20}$  value of the ImIBL model has a larger range of variation as compared with the BUU model. From the bottom panel of Fig.1, there is a bump in the early collision stage for BL model. But this phenomenon does not happen in the BUU simulations. This phenomenon suggests that there is a larger difference between the real quadrupole moment and averaged quadrupole moment, especially in the early collision stage. We think this phenomenon is important in the dynamical evolution process.

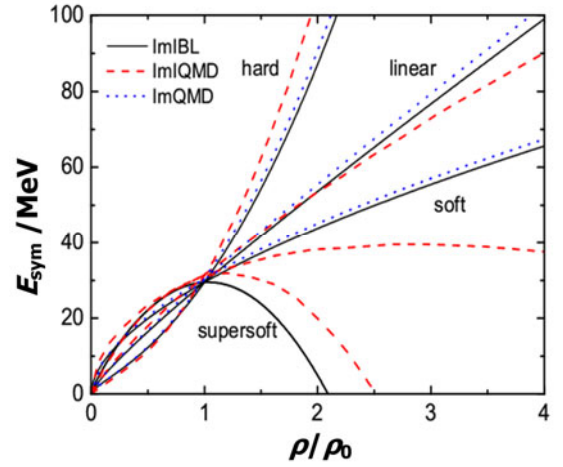


**Fig.2** (Color online) Symmetry energy as a function of the reduced density in this work (solid line), Ref.[8] (dashed line) and Ref.[14] (dotted line).

In the Vlasov part of Eq.(3), we work with an isospin and momentum dependent single nucleon potential, which reads

$$\begin{aligned}
 U_\tau(\rho, \delta, \vec{p}) &= \alpha \frac{\rho}{\rho_0} + \beta \left( \frac{\rho}{\rho_0} \right)^\gamma + E_{\text{sym}}^{\text{loc}}(\rho) \delta^2 \\
 &\quad + \frac{\partial E_{\text{sym}}^{\text{loc}}(\rho)}{\partial \rho} \rho \delta^2 + E_{\text{sym}}^{\text{loc}}(\rho) \rho \frac{\partial \delta^2}{\partial \rho_\tau} \\
 &\quad + U_{\text{MDI}},
 \end{aligned} \quad (7)$$

the bulk parameters  $\alpha$ ,  $\beta$ , and  $\gamma$  taken here are  $-390$  MeV,  $320$  MeV and  $1.14$  for the soft EOS plus MDI as SM and  $-130$  MeV,  $59$  MeV and  $2.09$  for the hard EOS plus MDI as HM<sup>[28]</sup>. The compressibilities  $K$  are  $200$  and  $380$  MeV for the SM and HM, respectively. The  $E_{\text{sym}}^{\text{loc}}(\rho)$ , which is the local part of the  $E_{\text{sym}}(\rho)$ , taken here are the following two forms

$$E_{\text{sym}}^{\text{loc}}(\rho) = \frac{1}{2} C_{\text{sym}} \left( \frac{\rho}{\rho_0} \right)^{\gamma_s} \quad (8)$$

and

$$E_{\text{sym}}^{\text{loc}}(\rho) = a \left( \frac{\rho}{\rho_0} \right) + b \left( \frac{\rho}{\rho_0} \right)^2 + c \left( \frac{\rho}{\rho_0} \right)^{5/3}. \quad (9)$$

In Eq.(8), the  $\gamma_s = 0.5, 1.0$  and  $2.0$  correspond to the soft, linear and hard symmetry energy respectively. The parameters  $C_{\text{sym}}, a, b$  and  $c$  are 33.4, 38.9, -18.9, and -3.8 MeV, respectively. Eq.(9) gives the supersoft symmetry energy. The curvature parameters  $K_{\text{sym}} = 9\rho_0^2 \left( \partial^2 E_{\text{sym}} / \partial \rho^2 \right) \Big|_{\rho_0}$  are 275.2, -25.4, -62.9, -403.6 MeV for the hard, linear, soft, and supersoft symmetry energy, respectively. Shown in Fig.2 is the comparison of the  $E_{\text{sym}}(\rho)$  for different cases from Eqs.(8) and (9), and also from the Refs.[8,14].

The momentum dependent potential can be expressed as<sup>[28]</sup>

$$U_{\text{MDI}} = 1.57 \ln^2 \left[ 0.0005 (\vec{p}_i - \vec{p}_j)^2 + 1 \right] \frac{\rho}{\rho_0}. \quad (10)$$

The inelastic channels and the parameterized cross sections of each channel are taken from Ref.[29]. We take the free space and in-medium cross sections for the elastic and inelastic channels, respectively. The in-medium effects are the medium correction of  $\rho$  mass<sup>[30]</sup>.

### 3 Results and discussion

#### 3.1 Neutron over proton ratio

Figure 3 shows the time evolution of the free neutron over proton ratio and the corresponding central point density in central  $^{48}\text{Ca}+^{48}\text{Ca}$  collisions at 400A MeV. The calculations are performed by using the supersoft and hard symmetry energies, respectively. The solid and dashed lines denote the results in the angle interval  $70^\circ < \theta < 110^\circ$  and in the rapidity interval  $-0.2 < y^0 < 0.2$ . The dotted and dotted-dashed lines show the results without any cuts.

From Fig.3, we can see that the supersoft behavior of the symmetry energy leads to a low neutron emission in the high-density region. In low-density region, an inversion of this trend is observed because of contributions to the nucleon emission in the expansion phase while fragments are forming. Our results are consistent with the one of Ref.[31].

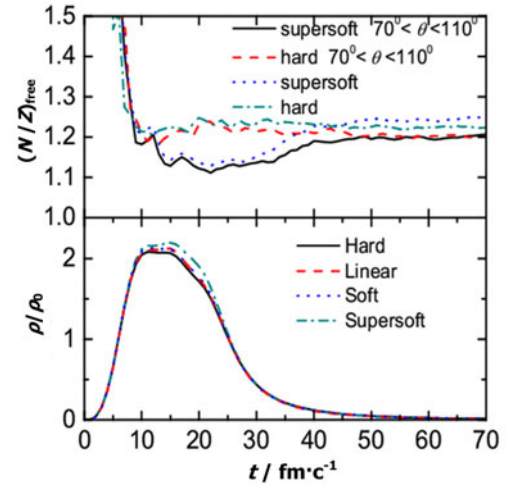


**Fig.3** (Color online) (Upper) Time evolution of free neutron over proton ratio for central  $^{48}\text{Ca}+^{48}\text{Ca}$  collisions at 400A MeV in the central rapidity and in the emission angle interval as indicated. (Bottom) Time evolution of the corresponding central point density.

#### 3.2 Pion multiplicity

In the left panel of Fig.4, we show the time evolution of  $\pi^\pm$  multiplicity in central  $^{48}\text{Ca}+^{48}\text{Ca}$  collisions at 400A MeV. The calculations are performed by taking four different forms of the  $E_{\text{sym}}(\rho)$ . From the left panel of Fig.4 and the bottom panel of Fig.3, one can see that the  $\pi$  is mainly produced in the high density region. Therefore, the  $\pi$  production will take useful information of the high density phase space. Most interestingly, the produced  $\pi^-$  is more sensitive to the  $E_{\text{sym}}(\rho)$  than the  $\pi^+$ . In order to further shed light on this point, we show in the right panel of Fig.4 the  $\pi^\pm$  multiplicity as a function of the curvature parameter  $K_{\text{sym}}$ . From the right panel of Fig.5, we can see that the  $\pi^-$  yield strongly varies with different  $E_{\text{sym}}(\rho)$  from soft to stiff case. This is because the  $\pi^-$  is mainly produced in neutron-neutron collisions. In the high density region a softer  $E_{\text{sym}}(\rho)$  will result in a low neutron emission, and then there will be more neutron rich as compared with the case of a hard  $E_{\text{sym}}(\rho)$ . We can conclude that the  $\pi^-$  yield play an important role in investigating the  $E_{\text{sym}}(\rho)$ .

#### 3.3 $\pi^-/\pi^+$ ratio

To further understand the dependence of the  $E_{\text{sym}}(\rho)$  on the  $\pi$  production, we show in Fig.5 the differential  $\pi^-/\pi^+$  ratios as functions of the kinetic energy and transverse momentum in the  $^{48}\text{Ca}+^{48}\text{Ca}$  collisions at 400A MeV with the impact parameter

$b=1$  fm. One can see that in the low energy and low transverse momentum regions the  $\pi^-/\pi^+$  ratio is very sensitive to the  $E_{\text{sym}}(\rho)$ . Therefore, we do not need to measure the high energy and high transverse momentum pions to constrain the density dependence of the symmetry energy. This will be useful in designing the experimental facilities with an aim of investigating the density dependent symmetry energy. From Fig.5, it is found that a supersoft symmetry energy results in a larger  $\pi^-/\pi^+$  ratio, which is consistent with the results of Refs.[7,9] and inconsistent with the one of Refs.[8,10].

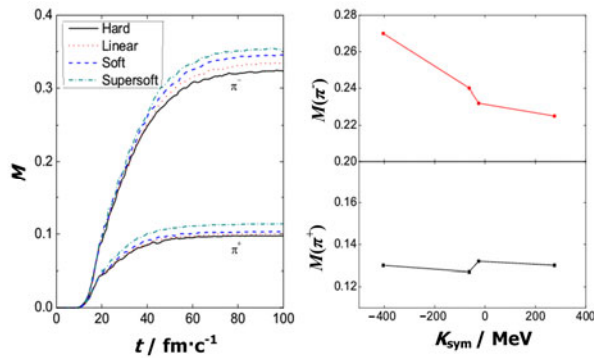


**Fig.4** (Color online) (Left) Time evolution of  $\pi^\pm$  multiplicity and (Right) the  $\pi^\pm$  multiplicity as a function of the  $K_{\text{sym}}$  in the  $^{48}\text{Ca}+^{48}\text{Ca}$  collisions at 400A MeV with the impact parameter  $b=1$  fm.

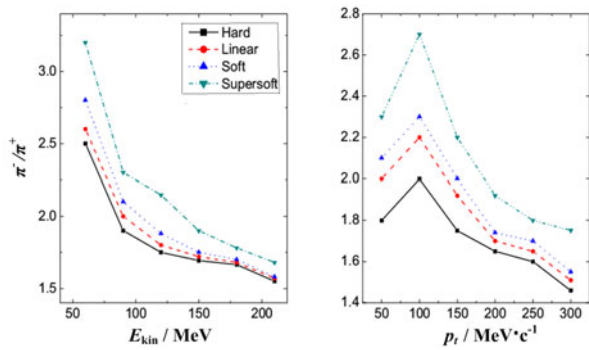


**Fig.5** (Color online) (Left) Kinetic energy spectra and (Right) transverse momentum spectra of the  $\pi^-/\pi^+$  ratio for the  $^{48}\text{Ca}+^{48}\text{Ca}$  collisions at 400A MeV with the impact parameter  $b=1$  fm.

#### 4 Conclusion

In summary, the  $E_{\text{sym}}(\rho)$  has been investigated by using the free neutron over proton ratio and the  $\pi$  production in the  $^{48}\text{Ca}+^{48}\text{Ca}$  collisions at 400A MeV in the framework of ImIBL model. It is found that both the free neutron over proton ratio and the  $\pi^-/\pi^+$  ratio are sensitive to the  $E_{\text{sym}}(\rho)$ . A soft  $E_{\text{sym}}(\rho)$  results in

a low emission of neutron component in the high density region. The  $\pi^-$  yield is strongly dependent on the  $E_{\text{sym}}(\rho)$  and the  $\pi^+$  yield is almost independent on the  $E_{\text{sym}}(\rho)$ . The  $\pi^-/\pi^+$  ratio in the low kinetic energy and low transverse momentum region is sufficient to constrain the  $E_{\text{sym}}(\rho)$ . The  $\pi^-/\pi^+$  ratio becomes larger when the  $E_{\text{sym}}(\rho)$  varies from the stiff to the soft.

Meson production as a probe of the  $E_{\text{sym}}(\rho)$  is still an open question. It is known that the threshold effect is important in the  $K$  meson production. For  $\pi$  meson, the threshold effect, which is not concluded in the present calculations, may also play an important role in the whole evolution stage. We will incorporate the threshold effect into the ImIBL model in the future work.

#### References

- 1 Li B A, Chen L W, Ko C M. Phys Rep, 2008, **464**: 113–281.
- 2 Danielewicz P and Lee J. Nucl Phys A, 2009, **818**: 36–96.
- 3 Zhang F S and Chen L W. Chin Phys Lett, 2001, **18**: 142–144.
- 4 Yong G C, Li B A, Chen L W. Phys Lett B, 2007, **650**: 344–347.
- 5 Li B A. Phys Rev Lett, 2002, **88**: 192701.
- 6 Li B A, Yong G C, Zuo W. Phys Rev C, 2005, **71**: 014608.
- 7 Xiao Z G, Li B A, Chen L W, *et al.* Phys Rev Lett, 2009, **102**: 062502.
- 8 Feng Z Q and Jin G M. Phys Lett B, 2010, **683**: 140–144.
- 9 Xie W J, Su J, Zhu L, *et al.* Phys Lett B, 2013, **718**: 1510–1514.
- 10 Ferini G, Gaitanos T, Colonna M, *et al.* Phys Rev Lett, 2006, **97**: 202301.
- 11 Li Q F, Li Z X, Zhao E G, *et al.* Phys Rev C, 2005, **71**: 054907.
- 12 Stock R. Phys Rep, 1986, **135**: 259–315.
- 13 Reisdorf W, Stockmeier M, Andronic A, *et al.* Nucl Phys A, 2007, **781**: 459–508.
- 14 Tsang M B, Zhang Y, Danielewicz P, *et al.* Phys Rev Lett, 2009, **102**: 122701.
- 15 Chen L W, Ko C M, Li B A. Phys Rev Lett, 2005, **94**: 032701.
- 16 Centelles M, Roca-Maza X, Viñas X, *et al.* Phys Rev Lett, 2009, **102**: 122502.

- 17 Kumar S, Ma Y G, Zhang G Q, *et al.* Phys Rev C, 2011, **84**: 044620.
- 18 Li B A, Ko C M, Ren Z Z. Phys Rev Lett, 1997, **78**: 1644–1647.
- 19 Zhang Y X, Danielewicz P, Famiano M, *et al.* Phys Lett B, 2008, **664**: 145–148.
- 20 Li B A, Chen L W, Yong G C, *et al.* Phys Lett B, 2006, **634**: 378–382.
- 21 Amorini F, Cardella G, Giuliani G, *et al.* Phys Rev Lett, 2009, **102**: 112701.
- 22 Natowitz J B, Röpke G, Typel S, *et al.* Phys Rev Lett, 2010, **104**: 202501.
- 23 Germain M, Hartnack Ch, Laville J L, *et al.* Phys Lett B, 1998, **437**: 19–23.
- 24 Abe Y, Ayik S, Reinhard P G, *et al.* Phys Rep, 1996, **275**: 49–196.
- 25 Zhang F S and Suraud E. Phys Rev C, 1995, **51**: 3201–3210.
- 26 Suraud E, Ayik S, Belkacem M, *et al.* Nucl Phys A, 1992, **542**: 141–158.
- 27 Suraud E, Ayik S, Belkacem M, *et al.* Nucl Phys A, 1994, **580**: 323–334.
- 28 Aichelin J. Phys Rep, 1991, **202**: 233–360.
- 29 Huber S and Aichelin J. Nucl Phys A, 1994, **573**: 587–625.
- 30 Li Q F, Li Z X, Mao G J. Phys Rev C, 2000, **62**: 014606.
- 31 Rizzo J, Colonna M, Di Toro M. Phys Rev C, 2005, **72**: 064609.